Time-lapse FWI using simultaneous sources

He Liu, Xin Fu, Daniel Trad, Kristopher Innanen

ABSTRACT

Full waveform inversion (FWI) has been used to estimate high-resolution subsurface velocity models. It has become a powerful tool for time-lapse seismic inversion, which is promising to monitor reservoir profile changes with injection and production, and potentially long-term storage of CO_2. To overcome the challenge of expensive computational costs for FWI processes, shot subsampling methods and source-encoding strategies have been used to make the full waveform inversion efficient while maintaining the quality of the inversion results with minimum sacrifice. The cyclic method subsamples the shots at a regular interval and changes the shot subset at each iteration step. Using this method, we can suppress the aliasing noise present in regular-interval subsampling. FWI using source-encoding strategies has been investigated using different methods. In previous work, we have used an amplitude-encoding strategy with different bases to accelerate the FWI process. In this work, we incorporate an amplitude-encoding strategy with a cyclic subsampled data scheme, which first subsamples the data cyclically and then composes blended during the iterations. In this way, we can directly eliminate much more crosstalk terms introduced by encoded individual shot gathers and reduce the data dimension to improve FWI efficiency. We have applied this strategy to acoustic and elastic time-lapse FWI in the time domain, and the synthetic inversion results recovered the velocity profile changes in the time-lapse models very well with reduced computation efforts.

INTRODUCTION

The classical time-domain FWI was originally proposed by Tarantola (1984) to invert the velocity model by minimizing the l2-norm of the difference between predicted and observed data (Symes, 2008, Virieux et al., 2017). This technique has become a powerful tool for time-lapse inversion and promising in monitoring reservoir change with time. However, FWI suffers from a heavy computational burden. To make FWI more efficient, source-encoding strategies have been proposed (Romero et al., 2000; Krebs et al., 2009, Schuster et al., 2011, Liu et al, 2021), which reduce the data dimension by encoding the individual shot gathers into super-shots. We have applied the amplitude-encoding strategy (Godwin and Sava, 2013; Hu et al., 2016) to acoustic and elastic FWI, which assigns different weights to the shot gathers to compose multiple super-shots.

However, when the number of super-shots is small, the introduced crosstalk noise between all the individual shots within the super-shots is still significant.

Alternatively, shot subsampling or shot decimation techniques can be used to attain efficiency in a full waveform inversion (Díaz and Guitton, 2011; van Leeuwen et al., 2011; van Leeuwen and Herrmann., 2012; Li et al., 2012; Ha and Shin, 2013). These techniques use a small number of chosen shot gathers to reduce the computation time with no extra crosstalk noise introduced. However, to make sure the information from chosen shots is adequate for FWI, the number of shots used in the inversion should be not too small and the reduction of data dimension is limited.

In this work, we use an amplitude-encoding strategy to blend subsampled shot gathers into super-shots. In this way, after we chose adequate shot gathers to recover subsurface structures, we can further reduce data dimension, and the number of crosstalk terms introduced by the encoding scheme could be significantly reduced compared with using all the individual shots. To extrude the impact of the time-lapse inversion strategy, we use a common parallel strategy (PRS) and apply the subsampled data-based amplitude-encoding scheme to both acoustic and elastic time-lapse FWI. Examples using down-sampled synthetic data obtained from the Marmousi model show good results.

In this report, we first introduce the schemes of data subsampling and amplitude-encoding, then demonstrate the feasibility of our scheme with the synthetic examples of both acoustic and elastic FWI using down-sampled Marmousi models.

SUBSAMPLING THE SHOTS

The simplest subsampling method is regular subsampling, which statically subsamples every nth specific shot shown in Figure 1a. Since some of the information in the observed data is lost, this scheme degrades the inversion result. To better take the advantage of data information, random subsampling (Díaz and Guitton, 2011) and cyclic subsampling (Ha and Shin, 2013) have been proposed. Although the probability of a shot being used is the same, the actual number of assignments can vary for each shot in the random subsampling methods shown in Figure 1b. Alternatively, a cyclic subsampling method uses every shot the same number of times or at least a similar number of times (Figure 1c). To avoid distance variability between the selected shots, the selected shots in each subgroup are uniformly spaced.

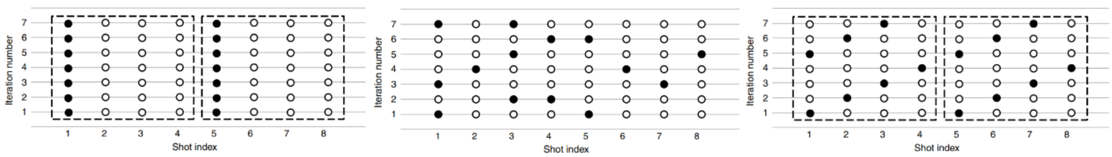

Figure 1. The regular, random and cyclic subsampling schemes. The black dots indicate the shots used in an iteration (adopted from Ha and Shin, 2013).

AMPLITUDE-ENCODING FWI

We review this strategy in an acoustic case with constant density, the acoustic wave equation is described by Yang et al. (2014)

$$\frac{1}{\mathrm{v}^2(\mathrm{x})}\ \frac{\partial^2\,\mathrm{p}(\mathrm{x},\ \mathrm{t}\,;\ \mathrm{x_s})}{\partial\,\mathrm{t}^2} - \nabla^2\,\mathrm{p}(\mathrm{x},\ \mathrm{t}\,;\ \mathrm{x_s}) = \mathrm{f_s}(\mathrm{x},\ \mathrm{t}\,;\ \mathrm{x_s})$$

where fs is the source term. The objective function (data misfit function) of $\Delta\mathbf{p}$ is given by

$$E(\boldsymbol{m}) = \frac{1}{2}\boldsymbol{\Delta}\mathbf{p}^{\dagger}\boldsymbol{\Delta}\mathbf{p} = \frac{1}{2}||\mathbf{p}_{\mathrm{cal}} - \mathbf{p}_{\mathrm{obs}}||^2$$

where † denotes the adjoint operator (conjugate transpose).

In encoding FWI, shot gathers are transformed into super shot gathers by the encoding matrix, which is defined as

$$\mathbf{B} = \begin{bmatrix} b^{1,1} & \cdots & b^{Nsig,1} \\ \vdots & \ddots & \vdots \\ b^{1,N_{sup}} & \cdots & b^{Nsig,N_{sup}} \end{bmatrix}_{N_{sup}\times N_{sig}}$$

where *Nsup* is the number of the super-shots and *Nsig* is the number of the individual shots (*Nsup* < *Nsig*). The *Nsig* synthetic data and observed data are blended into *Nsup* blended data by

$$\mathbf{p}_{\mathrm{cal}}^{\mathrm{sup}} = \mathbf{B}\mathbf{p}_{\mathrm{cal}}$$

$$\mathbf{p}_{\mathrm{obs}}^{\mathrm{sup}} = \mathbf{B}\mathbf{p}_{\mathrm{obs}}$$

The ratio between Nsig and Nsup is the factor by which the computational cost is reduced. Since usually Nsup is much smaller than Nsig, the encoding FWI would achieve much better efficiency due to the reduction of data dimension.

Then the encoding objective function is given by:

$$E(\mathbf{m}) = \frac{1}{2}\boldsymbol{\Delta}\mathbf{p}^{\dagger}\boldsymbol{\Delta}\mathbf{p} = \frac{1}{2}||\mathbf{p}_{\mathrm{cal}} - \mathbf{p}_{\mathrm{obs}}||^2 = \frac{1}{2}(p_{cal} - p_{obs})\mathbf{B}^{\mathrm{T}}\mathbf{B}(p_{cal} - p_{obs})$$

The matrix $\mathbf{B}^{\mathrm{T}}\mathbf{B}$ is referred to as the crosstalk matrix, and when it's equal to the identity matrix, the encoding objective function is equal to the traditional objective function. FWI using blended data would produce the same results as in conventional FWI cases. Therefore, to make the inversion result from the encoding FWI comparable to that from the conventional FWI, the designed encoding crosstalk matrix should be a good approximation of the identity matrix (Liu et al., 2021). In this work, we use a sine basis as the encoding matrix, which is defined as (Tsitsas, 2010):

$$\mathrm{b}_{m,n} = \sqrt{\frac{2}{n_{\mathrm{sig}}}} \sin\left(\frac{\left(m+\frac{1}{2}\right)\left(n+\frac{1}{2}\right)\pi}{n_{\mathrm{sig}}}\right)$$

TIME-LAPSE INVERSION STRATEGY

We use the parallel strategy (PRS) following the workflow in Figure 2. We invert the baseline and monitor models with the same initial model independently and obtain the inverted time-lapse model through the subtraction between two inversion results.

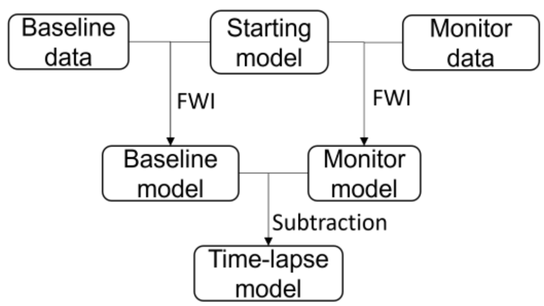

Figure 2. Flowchart of parallel strategy (PRS) of time-lapse FWI.

SYNTHETIC EXAMPLES

Down-sampled acoustic Marmousi model

In this section, we use a down-sampled acoustic Marmousi model to test the scheme. The true baseline model is shown in Figure 3a, two reservoirs are located left and right at mid-depth in the model, respectively. To mimic the fluid change, 150 m/s acoustic velocity changes, are added at the two reservoirs as displayed in Figure 3b to obtain the monitor model. A smoothed initial model is displayed in Figure 3c, which is used in FWI of both baseline and monitor models.

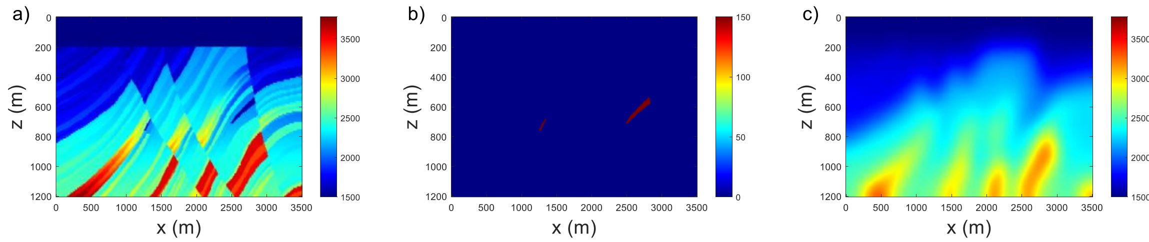

Figure 3: a) True baseline model. b) True time-lapse model. c) The starting model is obtained by smoothing the true baseline model.

The models have a distance of 3500 m and a depth of 1200 m and are discretized by 350 by 120 cells with 10 meters grid spacing. On the top of the model, 174 sources are evenly distributed at the depth of 20 m and 350 receivers are located at each grid point. The source wavelets used for baseline and monitor data sets are identical with a dominant frequency of 10 Hz. The time sampling interval is 1.5 ms and the maximum recording time is 2 s.

We subsample 58 shot gathers to compose 10 super-shots with even spatial distance from all 174 shots and re-subsample the data cyclically every few iterations. Using an amplitude-encoding strategy for all the individual shots, we can get the encoding and crosstalk matrices as shown in Figures 4a and 4c. From the crosstalk matrix, we can notice many non-zero elements off the main diagonal, which represent the coefficients of the crosstalk terms. After applying the cyclic subsampling scheme, we use 58 shots of all the observed data at each iteration to compose super-shots. In Figures 4b and 4d we see the encoding and crosstalk matrices at the first iteration. From the crosstalk matrix, we can notice that compared with Figure 4c, many off-diagonal elements are reduced to zero.

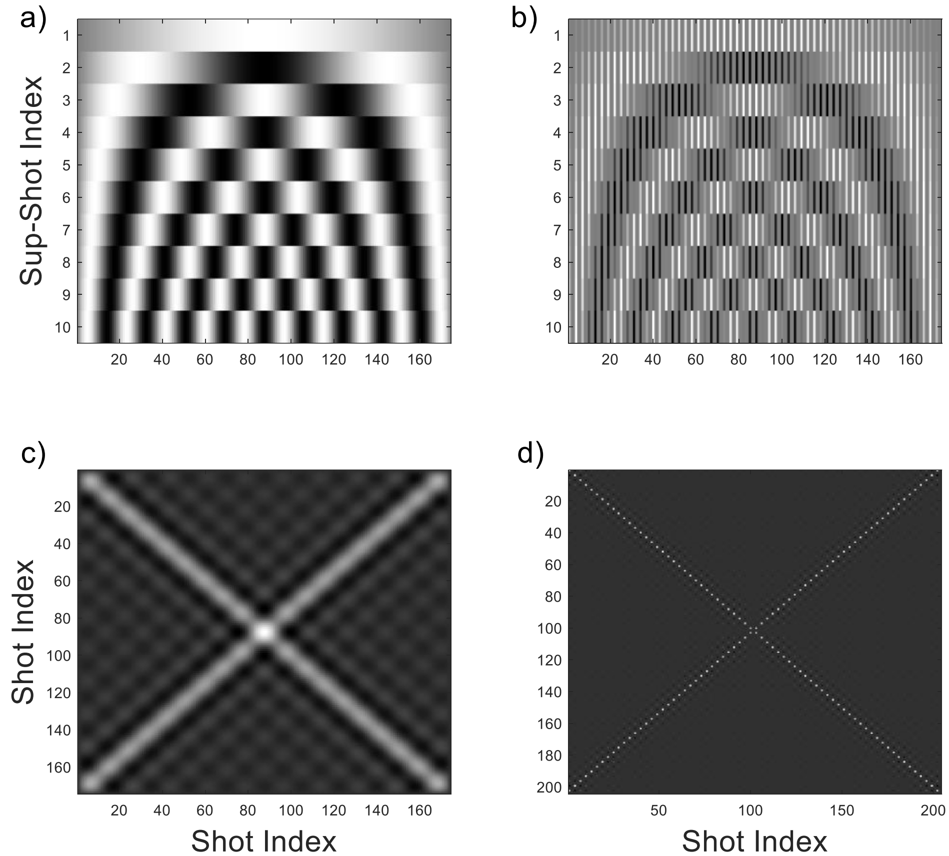

Figure 4: The encoding (first row) and crosstalk (second row) matrices: using all the individual shots (left column) and subsampled shots (right column).

To show the capacity of the time-domain constant-density acoustic FWI program used in this study, we first present the inverted baseline model in Figure 5a, and two vertical profiles through the two reservoirs at distances of 1300 m and 2700 m, which are extracted and plotted in Figure 5b. From the final image after 100 iterations shown in Figure 5a, we can see the fine subsurface structures in the Marmousi model are well recovered with no significant crosstalk noise introduced. In Figure 5b, we compare the inverted and true velocity profiles. In this Figure, the solid black lines are the true models, the dashed red lines are starting models, and the yellow lines are inverted baseline models. The reservoirs are located at 740 m and 600 m deep. From the comparison, we can see the black and yellow lines match very well, even though the fine structures at large depths need further updates.

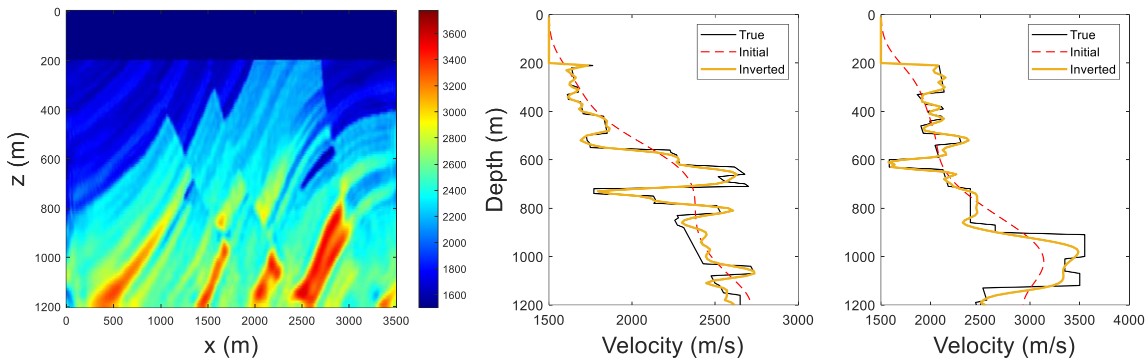

Figure 5. a) Inverted baseline model; b) The solid black lines are the true model, the dashed red lines are starting models, and the yellow lines are inverted baseline models at distance 1300 m (left) and 2700 m (right).

From the inverted baseline and monitor models, we see the technique does not introduce obvious crosstalk noises in the final images. Using a parallel time-lapse FWI strategy, we use the same scheme to invert the monitor model, which is shown in Figure 6b. We show the inverted time-lapse model after subtraction in Figure 6c. We can see the well-inverted velocity changes in the two reservoirs.

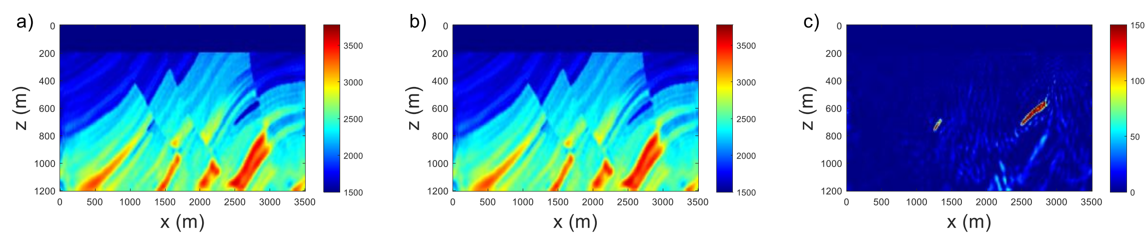

Figure 6: Inverted baseline, monitor and time-lapse models.

Down-sampled elastic Marmousi II model

In this section, we applied the scheme to elastic time-lapse FWI. We used a down-sampled elastic Marmousi II model with a distance of 4100 m and a depth of 1500 m in a grid of 410 by 150 cells with 10 meters size each. This model consists of a 200 m thick water layer above. In this work, we consider density constant and only perform FWI for Vp and Vs using the IFOS2D software (Bohlen, et al., 2016).

The true baseline Vp and Vs models are shown in Figures 7a and 7d. Figure 7b and 7e show the smoothed initial models for Vp and Vs. As in the acoustic case, we set two velocity change areas located at 600 m deep in the model. In the time-lapse model shown in Figures 7c and 7e, Vp change is also set to 150 m/s and Vs change is set to 89 m/s.

We deployed 204 sources and 410 receivers along the model surface at the depth of 20 m and 30 m, respectively. The source wavelets used for baseline and monitor data sets are identical with a dominant frequency of 10 Hz. The time sampling interval is 1.25 ms and the maximum recording time is 3 s.

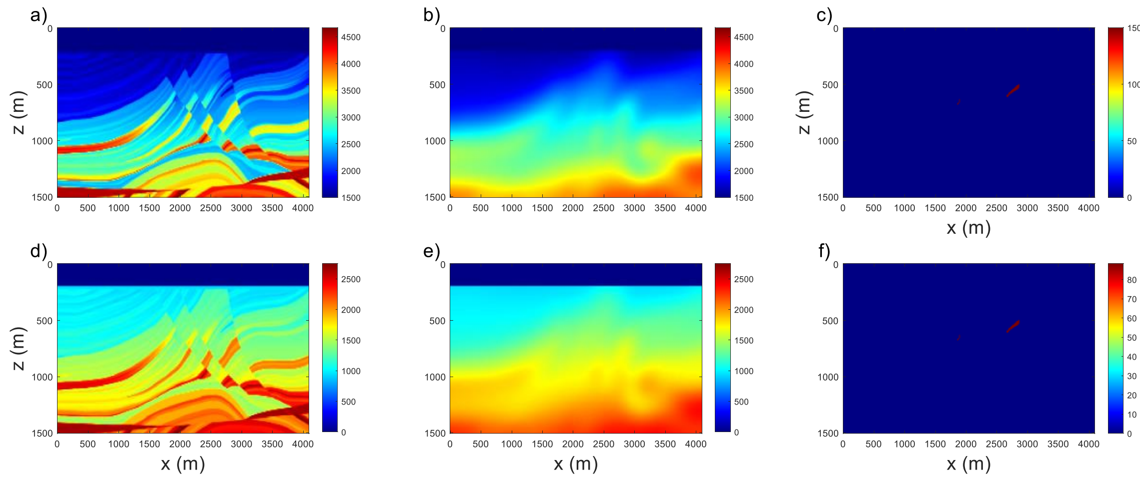

Fig 7. Down sampled Marmousi II model: columns from left to right are the true, initial and time-lapse Vp and Vs profiles.

In this experiment, we subsample every 3 shots and compose 40 super-shots. For comparison, we display the encoding and crosstalk matrices using all the individual and selected shot gathers in Fig 8.

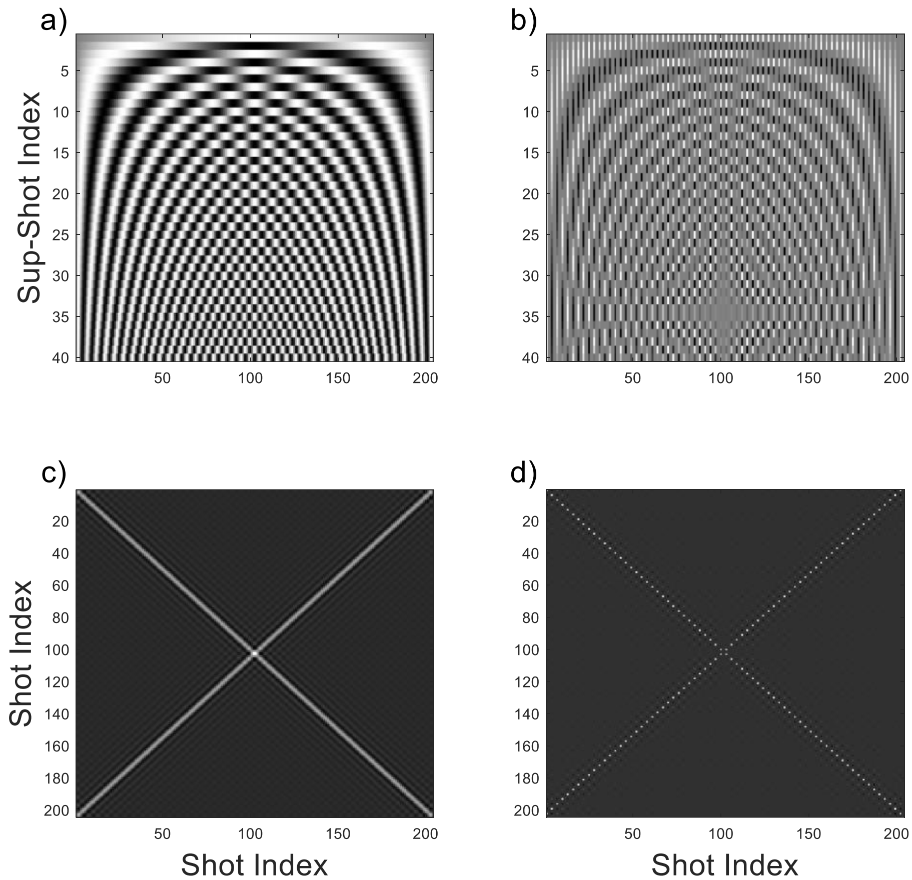

Figure 8: The encoding (first row) and crosstalk (second row) matrices: using all the individual shots (left column) and subsampled shots (right column).

For elastic FWI, we use a multi-scale approach and invert the baseline and monitor models from 1 Hz to 20 Hz. Also, we first present the inversion results for the baseline model. The final images and vertical profiles of Vp and Vs at two velocity change areas are shown in Figures 9 and 10, respectively.

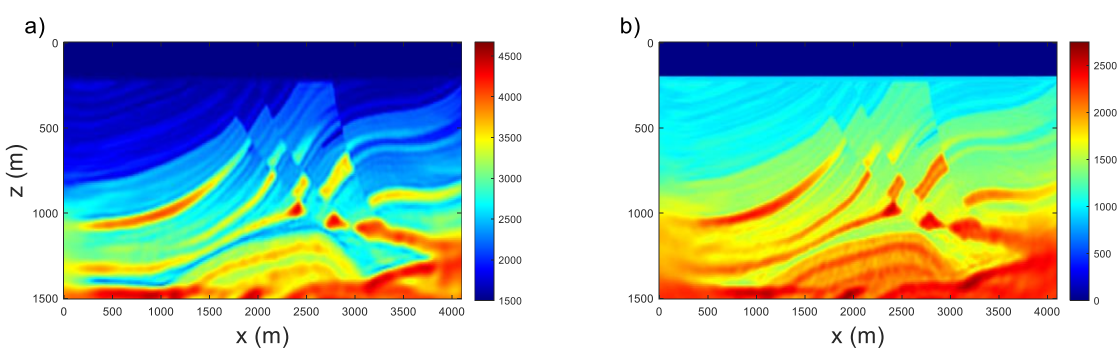

Figure 9. Inverted baseline model, a) Vp and b) Vs.

From Figure 9, we can see that amplitude-encoding elastic FWI based on subsampled data can produce high-quality inversion results with no obvious crosstalk noise introduced in the final images as in the acoustic case.

In Figure 10, vertical Vp (left) and Vs (right) profiles at 2.1 km and 3.0 km of the initial model and inversion results are compared with the true models. Within each panel, the black line is the true model and the dashed red line is the initial model, the yellow lines are the results of amplitude-encoding elastic FWI. We can see results contain small details and identify the fine layers with reduced calculation effort. Both of the velocity change areas are located at around 600 m deep, which are well resolved in Vp and Vs vertical profiles.

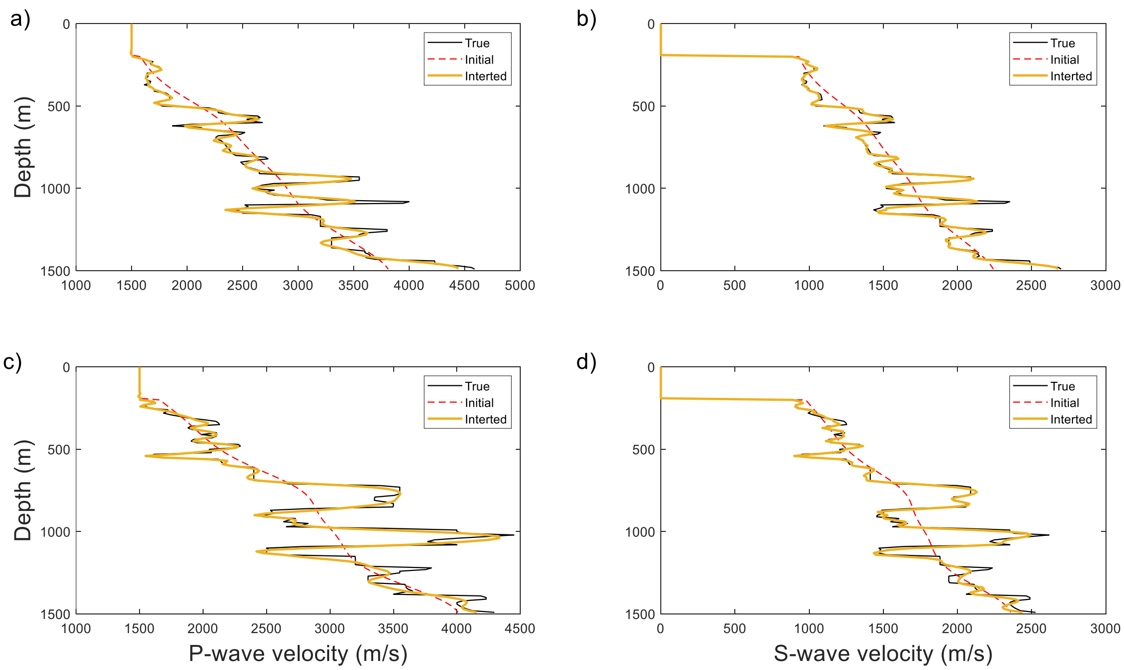

Figure 10: Vertical profiles of the elastic parameters within the reservoir areas extracted at distances 2.1 km and 3.0 km: a) and c) P-wave velocity, b) and d) S-wave velocity.

Then we use the same scheme to invert the monitor model. For comparison, both inverted baseline and monitor models are shown in the first and second columns in Figure 11. Last, subtracted time-lapse Vp and Vs models are displayed in Figures 11c and 11f, respectively.

Inverted time-lapse models are plotted at the same scale as the true models. From the result of Vp, we can see that except for some artifacts resulting from convergence differences between baseline and monitor models, the Vp changes within the two areas are well resolved.

Figure 11f shows the inverted time-lapse vs model. We can also see the Vs profile change is well-resolved for both areas. What is different is that at some high-velocity fine layers at a large depth around the bottom left and right corners of the model, the convergence difference between baseline and monitors models shows a bigger impact on the Vs profile, which may be better coped with advanced time-lapse inversion strategies, such as common model strategy (CMS) (Hicks et al., 2016; Fu and Innanen, 2021).

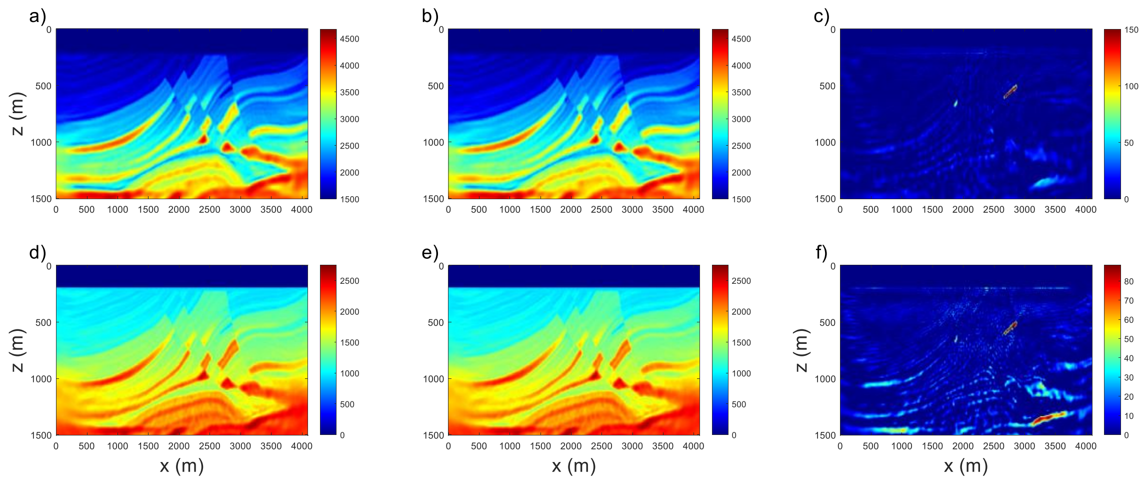

Figure 11. Inversion results for elastic parameters: columns from left to right are the baseline, monitor and time-lapse Vp and Vs profiles.

We further apply CMS strategy to the time-lapse inversion, the flowchart is shown in Figure 12. So we used the averaged inversion result as the initial model. Instead of using multi-scale approach to invert baseline and monitor models from 1 Hz all the way to 20 Hz, we stop the inversion if only the misfit stopping decreasing. Finally, The final time-lapse model is obtained from a difference of the baseline and monitor models, and the time-lapse inversion result comparison between two strategies are shown in Figure 13. b) and d) are Vp and Vs profiles by CMS. From the comparison, we can see the CMS strategy has better mitigated the artifacts.

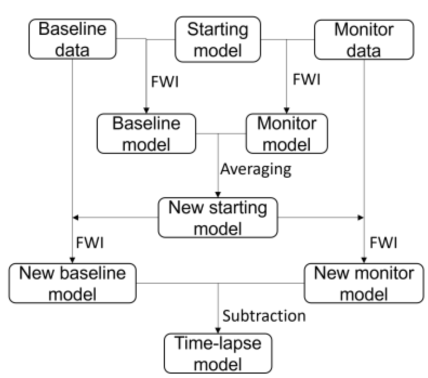

Figure 12. Flowchart of common-model strategy (CMS) of time-lapse FWI.

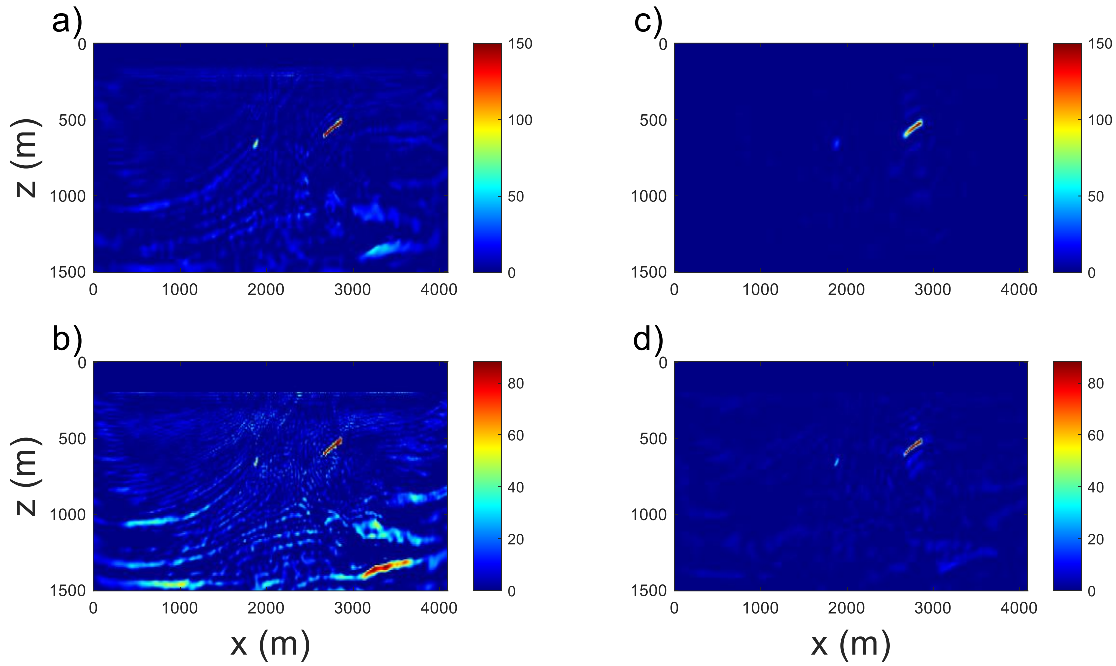

Figure 13. Inversion results for elastic parameters: a) and c) are Vp and Vs profiles by PRS;

CONCLUSIONS

We presented cyclic subsampled data-based amplitude-encoding time-lapse FWI in the time domain. FWI examples show that using amplitude-encoding with subsampled shots can make the inversion process efficient with minimum sacrifices in the inversion results. Based on subsampled shots, the number of crosstalk terms in the crosstalk matrix can be significantly reduced. We have applied this scheme to both acoustic and elastic time-lapse FWI, both synthetic examples show promising results. In addition, we applied common-model strategy to elastic time-lapse FWI and obtain time-lapse models with better mitigated artifacts.

ACKNOWLEDGEMENT

We thank the sponsors of CREWES for their continued support. This work was funded by CREWES industrial sponsors and NSERC (Natural Science and Engineering Research Council of Canada) through the grant CRDPJ 543578-19. We would also like to thank Dr. Pengliang Yang for his contribution to the acoustic FWI program and the developers of the software IFOS2D.

REFERENCES

Bohlen, T., Nil, D., Groos, L., Heider, S., Köhn, D., Kurzmann, A., Schaefer, M., Gassner, L., Metz, T., Thiel, N. et al., 2016, Ifos2d, version 2.0. 3.

Dai, W., Fowler, P., and Schuster, G. T., 2012, Multi-source least-squares reverse time migration: Geophysical Prospecting, 60, No. 4-Simultaneous Source Methods for Seismic Data, 681–695.

Díaz, E., and A. Guitton, 2011, Fast full waveform inversion with random shot decimation: 81st Annual International Meeting, SEG, Expanded Abstracts, 2804–2808.

Fu, Xin, and Innanen, Kristopher., 2021, Stepsize sharing in time-lapse full-waveform inversion, CREWES annual report, 2021, volume 34.

Florez, K. A., Mantilla, J. G., and Ramirez, A. B., 2016, Full waveform inversion (fwi) in time for seismic data acquired using a blended geometry, in 2016 XXI Symposium on Signal Processing, Images and Artificial Vision (STSIVA), IEEE, 1–5.

Godwin, J., and Sava, P., 2013, A comparison of shot-encoding schemes for wave-equation migration: Geophysical Prospecting, 61, 391–408.

Ha, W., and Shin, C., 2013, Efficient Laplace-domain full waveform inversion using a cyclic shot subsampling method: Geophysics, 78(2), R37-R46.

Hu, J., Wang, H., Fang, Z., Li, T., and Zhang, J., 2016, Efficient amplitude encoding least-squares reverse time migration using cosine basis: Geophysical prospecting, 64, No. 6, 1483–1497.

Hicks, E., Hoeber, H., Houbiers, M., Lescoffit, S. P., Ratcliffe, A., and Vinje, V., 2016, Time-lapse full waveform inversion as a reservoir-monitoring tool—a north sea case study: The Leading Edge, 35, No. 10, 850–858.

Krebs, J. R., Anderson, J. E., Hinkley, D., Neelamani, R., Lee, S., Baumstein, A., and Lacasse, M.-D., 2009, Fast full-wavefield seismic inversion using encoded sources: Geophysics, 74, No. 6, WCC177–WCC188.

Romero, L. A., Ghiglia, D. C., Ober, C. C., and Morton, S. A., 2000, Phase encoding of shot records in prestack migration: Geophysics, 65, No. 2, 426–436.

Symes, W. W., 2008, Migration velocity analysis and waveform inversion: Geophysical prospecting, 56, No. 6, 765–790.

Tarantola, A., 1984, Inversion of seismic reflection data in the acoustic approximation: Geophysics, 49, No. 8, 1259–1266.

Tsitsas, N. L., 2010, On block matrices associated with discrete trigonometric transforms and their use in the theory of wave propagation: Journal of Computational Mathematics, 864–878.

Virieux, J., Asnaashari, A., Brossier, R., Métivier, L., Ribodetti, A., and Zhou, W., 2017, An introduction to full waveform inversion, in Encyclopedia of exploration geophysics, Society of Exploration Geophysicists, R1–1.

van Leeuwen, T., M. Schmidt, M. Friedlander, and F. Herrmann, 2011, A hybrid stochastic-deterministic optimization method for waveform inversion: 73rd Annual International Conference and Exhibition, EAGE, Extended Abstracts, 1595–1599.

van Leeuwen, T., and F. Herrmann, 2012, Fast waveform inversion without source-encoding: Geophysical Prospecting, published online.

Yang, P., Gao, J., and Wang, B., 2015, A graphics processing unit implementation of time-domain full waveform inversion: Geophysics, 80, No. 3, F31–F39.